Switching time and energy in bistable injection-locked semiconductor multi-quantum-well Fabry-Perot lasers

M. M. Krstić, J. V. Crnjanski, and D. M. Gvozdić*
School of Electrical Engineering, University of Belgrade, Serbia
(Received 1 September 2013; published 12 December 2013)

In this paper, we investigate the influence of the linewidth enhancement factor and active region volume on the switching characteristics of bistable injection-locked multi-quantum-well Fabry-Perot lasers. In this analysis we start from the full scale model of the multimode rate equation system describing dynamics of injection-locked lasers. On the basis of this model, we derive a simple analytical procedure for calculation of switching time and energy with respect to the injection power, and for different values of frequency detuning between the master and the slave laser. We find that the higher values of linewidth and active region volume can improve switching characteristics of injection-locked Fabry-Perot lasers, providing either shorter switching times (∼10 ps) or lower switching energies (∼1 fJ).

DOI: 10.1103/PhysRevA.88.063826 PACS number(s): 42.65.Pc, 42.55.Px

I. INTRODUCTION

Injection locking is a nonlinear phenomenon [1,2] which has recently emerged as an attractive solution for low-cost upstream transmission in passive optical networks [3,4]. However, due to optically nonlinear and bistable output, injection-locked laser configurations can be also employed in digital optical signal-processing systems, such as optical switches [5], fast low-power memories [6], and all-optical flip flops [7] or regenerators [8], all representing hot research topics. Since recently, these effects are intensively studied in nanostructure lasers [9]. So far, several mechanisms behind the injection-locked (IL) bistability have been found and implemented in various applications. One of the recently exploited mechanisms for fabrication of all-optical flip flops is based on gain clamping and spatial hole burning [8,10], and thus may represent a kind of absorptive or gain-controlled bistability mechanism. The switching time achieved by this technique is about 250 ps, while the switching energy is about 500 fJ [10]. On the other hand, it has been shown in [11,12] that due to the dispersive bistability of IL lasers predicted by Lang [13], slave laser (SL) may exhibit up to three stationary states, two of which can be stable in a certain range of injection power P_{inj} and frequency detuning $\Delta\omega$ between the master and the slave laser. It has been pointed out in [11,12] that bistability significantly depends on the interaction between the IL mode and other, unlocked modes, therefore a detailed model, which takes into account all supported modes has been applied and recommended [11]. Switching between these two stable states can be achieved either by variation of P_{inj} or $\Delta\omega$ [14]. However, one of the most important remaining problems is poorly investigated switching speed and switching energy efficiency. So far, switching time in bistable laser diodes has been studied in the dependence on P_{inj} or $\Delta\omega$ [14], while earlier works had been focused on the switching achieved by the bias current variation [15].

A possible approach to calculate switching time is based on numerical solving of the full scale rate equation model in the transient regime. In addition to the IL mode, this model comprises equations for all other, unlocked modes. Although computationally demanding, such approach provides a precise method to investigate the influence of P_{inj} and $\Delta\omega$ variation on the switching from one (initial) to the other (final) stable state and its corresponding time (t_{if}) and energy (E_{if}). However, in [14] we have proposed a simple analytical formula for switching time prediction, which can provide an insight into switching time dependence on the P_{inj} or $\Delta\omega$ variation. The implementation of the formula in this paper is based on the stationary solutions of the full scale rate-equation model, which we use to derive the stationary hysteresis loops. Once the hysteresis loops and the stationary points are obtained, one can calculate t_{if} according to the derived analytical formula. If the switching is based on the variation of P_{inj}, it is possible to estimate E_{if}, as a product of the P_{inj} variation and t_{if}.

This paper provides an analysis of the switching time and energy versus P_{inj}, for various structural laser parameters and frequency detunings. Among parameters which may affect t_{if} and E_{if}, we focus our investigation on the linewidth enhancement factor (α), being directly responsible for the bistability effect, and the number of the quantum wells (N_w) in the active region, which determines the confinement factor and active region volume.

In Sec. II, we provide the theoretical background of the model based on the set of full scale rate equations describing the injection-locking phenomenon and all used parameters. Section III explains bistability induced by the injection locking and formation of hysteresis loop. In Sec. IV we present the analytical model for switching time and corresponding energy calculation. In Sec. V we deal with the analysis and the discussion of the results, and finally in Sec. VI we provide the conclusion of the paper.

II. THEORETICAL BACKGROUND

In our study we assume that the SL active region consists of a $In_{0.75}Ga_{0.25}As_{0.87}P_{0.13}$ (well) $In_{0.46}Ga_{0.39}Al_{0.15}As$ (barrier) 1.55 μm strain-compensated multi-quantum-well (QW) material. The QWs are considered weakly coupled or decoupled, which provide us with a possibility to study the optical properties of the active region by using material gain

*gvozdic@etf.bg.ac.rs

dependence on carrier and current density for a single well. The gain dependence $g(n,\omega)$ on carrier concentration n and photon angular frequency ω, as well as radiative spontaneous emission dependence $R_{sp}(n)$ on carrier concentration, are taken from [11]. In the free-running (FR) regime, the gain spectrum reaches its maximum at the threshold carrier concentration $n = n_{th}^{FR}$, and at the angular frequency $\omega = \omega_0$ corresponding to the central (dominant) mode. Due to the gain asymmetry with respect to ω, the number of side modes which can be supported by the laser cavity is different for $\omega < \omega_0$ (l_1) and for $\omega > \omega_0$ (l_2). The rate equation system comprises one equation regarding the carrier concentration (n) dynamics, $l_1 + l_2 + 1$ equations dealing with the time dependence of the photon concentration of the IL mode (S_m), and other unlocked longitudinal modes (S_j). The last equation describes the time evolution of the phase difference (θ_m) between the FR and IL states:

$$dn/dt = I/(qV) - Q(n) - \sum_{j=-l_1}^{l_2} v_g g(n,\omega_j) S_j, \tag{1}$$

$$dS_j/dt = A_j S_j + B(n), \qquad j \neq m, \tag{2}$$

$$dS_m/dt = A_m S_m + B(n) + 2k_c\sqrt{S_{inj} S_m}\cos\theta_m, \tag{3}$$

$$d\theta_m/dt = \alpha A_m/2 - \Delta\omega - k_c\sqrt{S_{inj}/S_m}\sin\theta_m. \tag{4}$$

In Eqs. (1)–(4) I stands for the bias current of the SL, V is the volume of its active area, corresponding to a laser width $w = 4$ μm, resonator length $L = 250$ μm, and N_w equally spaced QWs, with a well thickness of $d = 8.7$ nm. We define $Q(n)$ as the total recombination rate, representing the sum of the total spontaneous optical emission rate $R_{sp}(n)$ and nonradiative recombination rates, i.e., $Q(n) = A_{SRH}n + R_{sp}(n) + C_A n^3$, where $A_{SRH} = 1.1 \times 10^8$ s^{-1} [11] and $C_A = 5.82 \times 10^{-29}$ cm^6 s^{-1} [11] are the Shockley-Reed-Hall and the Auger recombination rate coefficients, respectively. For brevity and further clarifications, we define two additional auxiliary variables: the effective spontaneous emission $B(n) = \Gamma\beta_{sp}R_{sp}(n)$, and the effective rate of stimulated photon generation $A_j(n,\omega_j) = \Gamma v_g g(n,\omega_j) - \tau_p^{-1}$ for mode j, and $A_m(n,\omega_m) = \Gamma v_g g(n,\omega_m + \Delta\omega) - \tau_p^{-1}$ for the IL mode m. Frequency ω_j is the frequency of a side mode j, defined as $\omega_j = \omega_0 + j(\pi c/n_g L)$. In these expressions, v_g stands for the group velocity with $n_g = 4.2$, $\tau_p = (\Gamma v_g g_{th})^{-1}$ is the photon lifetime, Γ is the confinement factor calculated as $N_w \times \Gamma_1$, where $\Gamma_1 = 0.0187$ is the confinement factor per well, and the parameter β_{sp} is the spontaneous emission coupling factor [11]. For all modes in the FR regime $B(n) > 0$, while $A_j(n) < 0$ except for the central mode $j = 0$, for which $A_j(n_{th}^{FR}) = 0$. Furthermore, $k_c = 1.13 \times 10^{11}$ s^{-1} is the external light coupling factor [11], α is the linewidth enhancement factor, $\Delta\omega$ is the frequency detuning between master and slave lasers, and S_{inj} is the photon density which is proportional to P_{inj} and is given by $S_{inj} = \tau_p\Gamma P_{inj}/(\eta_0\hbar\omega V)$, where $\eta_0 = 0.33$ is the optical efficiency [11]. Frequency detuning of $\Delta\omega$ into the side mode m means that the frequency of the injected light is $\omega_{inj} = \omega_0 + m(\pi c/n_g L) + \Delta\omega$.

In our analysis we investigate the stationary solutions of Eqs. (1)–(4) in the dn/dt versus n space (or phase plot). From the stationary forms of Eqs. (3) and (4), by eliminating phase θ_m we obtain a quadratic equation with respect to stationary IL mode photon density S_m:

$$\left[A_m^2 + 4(\alpha A_m/2 - \Delta\omega)^2\right]S_m^2 + \left(2A_m B - 4k_c^2 S_{inj}\right)S_m + B^2 = 0, \tag{5}$$

for which a physically justified solution is given by

$$S_m = -\left\{\left(2A_m B - 4k_c^2 S_{inj}\right) + \sqrt{\left(2A_m B - 4k_c^2 S_{inj}\right)^2 - 4B^2\left[A_m^2 + 4(\alpha A_m/2 - \Delta\omega)^2\right]}\right\} \times \left\{2\left[A_m^2 + 4(\alpha A_m/2 - \Delta\omega)^2\right]\right\}^{-1}. \tag{6}$$

From the stationary form of Eq. (2) we derive $S_j = -B(n)/A_j(n)$, and substitute S_j and S_m in the stationary form of Eq. (1), obtaining a transcendental equation with respect to n:

$$I/(qV) - Q(n) + \sum_{-l_1 \leqslant j \leqslant l_2}^{j \neq m} v_g g(n,\omega_j) B(n)/A_j(n) - v_g g(n,\omega_m + \Delta\omega) S_m = 0, \tag{7}$$

in which S_m is given with Eq. (6). From Eq. (7) it is possible to find stationary carrier concentrations corresponding to the stationary states of the slave laser as well as hysteresis loops related to the bistability effect.

III. BISTABILITY AND HYSTERESIS LOOPS

In order to provide an insight into derivation of the hysteresis loops and the analytical expression for the switching time, we study a set of dn/dt versus n phase plots for a fixed $\Delta\omega = -14\Omega$ ($\Omega = 10^{10}$ rad/s), $\alpha = 3$, $N_w = 3$, and for different values of P_{inj} [Fig. 1(a)]. In this case, the number of supported modes is $l_1 + l_2 + 1 = 120 + 170 + 1 = 291$ and all of them are included into calculation. The injection is into the 5th mode from the central mode ($\hbar\omega_0 = 0.8$ eV) on the long-wavelength spectrum side, i.e. $m = -5$. We have shown in [11] that photon density of the IL mode S_m exhibits a maximum at carrier concentrations n lower than the threshold concentration for FR laser, n_{th}^{FR}, therefore, for a fixed negative detuning, depending on the magnitude of P_{inj}, dn/dt versus n phase plots may have up to three stationary points [Fig. 1(a)], i.e., Eq. (7) can have up to three solutions. In the range of moderate injection powers (-7.1 dBm $< P_{inj} < -2.4$ dBm), dn/dt versus n phase plots have three steady states [hatched region in Fig. 1(a)], which we denote as $n_{sp}^{(1)}$ (open circles, e.g., points 4, 5, and 6), $n_{sp}^{(2)}$ (crossed square), and $n_{sp}^{(3)}$ (filled circles, e.g., points 1, 2, and 3) in the increasing order of their values. For the lower range limit ($P_{inj} = -7.1$ dBm) $n_{sp}^{(2)}$ merges with $n_{sp}^{(1)}$ (point 6), while for the upper range limit ($P_{inj} = -2.4$ dBm) $n_{sp}^{(2)}$ merges with $n_{sp}^{(3)}$ (point 3). Stability analysis shows that $n_{sp}^{(2)}$ is always unstable [11,12], while depending on $\Delta\omega$ there is some moderate range of P_{inj} for which $n_{sp}^{(1)}$ and $n_{sp}^{(3)}$ are stable (e.g., for $\Delta\omega = -14\Omega$, P_{inj} range is from -7.1 to -2.4 dBm), providing the SL bistability [12]. Thus, once P_{inj} is increased to overcome -7.1 dBm,

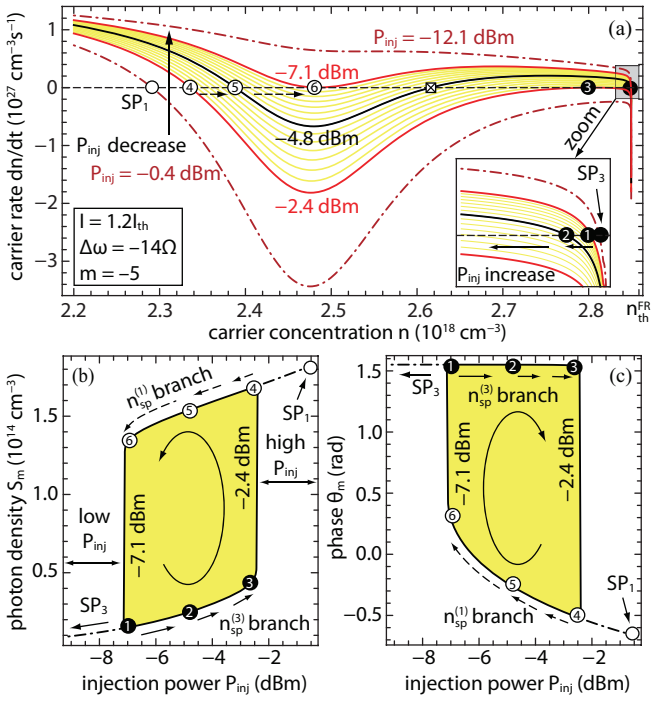

FIG. 1. (Color online) (a) dn/dt versus n phase plot for fixed $\Delta\omega = -14\Omega$, $N_w = 3$, $\alpha = 3$, and various P_{inj}, with all modes included. The hatched area represents the set of phase plots which have three stationary points: $n_{sp}^{(1)}$ (points 4, 5, and 6), $n_{sp}^{(2)}$, and $n_{sp}^{(3)}$ (points 1, 2, and 3). Dot-dashed curves represent situations with only one stationary point (point SP_3 for low P_{inj} and point SP_1 for high P_{inj}). Inset: Zoom of the area close to the n_{th}^{FR}. (b) Photon density of IL mode S_m versus P_{inj} and (c) IL mode phase θ_m versus P_{inj} hysteresis loop corresponding to (a). Dot-dashed tail parts of the hysteresis loops correspond to the phase plots with only one stationary point, while vertical boundaries correspond to the limiting cases, when $n_{sp}^{(2)}$ merges with $n_{sp}^{(1)}$ ($P_{inj} = -7.1$ dBm), and with $n_{sp}^{(3)}$ ($P_{inj} = -2.4$ dBm).

or decreased below -2.4 dBm, the SL enters the region of bistability.

For sufficiently low ($P_{inj} < -7.1$ dBm) or sufficiently high ($P_{inj} > -2.4$ dBm) injection power, the phase plot has only one stationary point. In the case of low P_{inj}, this stationary point is close to the n_{th}^{FR} [SP_3 point in the zoom inset in Fig. 1(a)] and becomes $n_{sp}^{(3)}$ with an increase in P_{inj}. Being close to the n_{th}^{FR}, such carrier concentration corresponds to the considerable emission from the dominant mode $j = 0$ and its closest side modes, while the emission from the IL mode is suppressed, i.e., the situation resembles the FR regime. Looking the other way around, one can conclude that the interplay between the IL and other, unlocked modes, determines the carrier concentration of SP_3 and $n_{sp}^{(3)}$ (i.e., its position in the phase plot). Although the emission from the dominant mode $j = 0$ and its closest side modes for this stationary point is significant, it is much smaller than the one corresponding to the FR regime or the one from the IL mode for higher P_{inj} [11]. This fact represents one of the important bases for our switching model. Since the carrier concentration for this stationary point is close to the FR regime, for which the IL mode is far from its maximum emission, the power output at wavelength corresponding to the injected light, i.e., IL mode, is low. For higher P_{inj}, S_m increases and exhibits a maximum corresponding to lower carrier concentrations than n_{th}^{FR}. The increase in S_m, especially its maximum, leads to the bending of dn/dt versus n plots toward the negative values of dn/dt [cf. Fig. 1(a)] providing simultaneously two additional stationary points ($n_{sp}^{(1)}$ and $n_{sp}^{(2)}$). However, the stationary point $n_{sp}^{(1)}$ is the only stable point of these two. This point remains stable and, with further increase in P_{inj}, becomes the only stationary point [SP_1 point in the Fig. 1(a)], while the unstable stationary point $n_{sp}^{(2)}$ vanishes. The carrier concentrations corresponding to SP_1 and $n_{sp}^{(1)}$ provide significant emission from the IL mode, which in this case considerably overcomes the output power corresponding to the dominant mode ($j = 0$) and the other unlocked modes. The main reason for that is a high injection power into the IL mode.

The existence of two stable stationary points ($n_{sp}^{(1)}$ and $n_{sp}^{(3)}$) for a single P_{inj} and $\Delta\omega$ leads to the bistability. The bistability is related to the optical power hysteresis loop at the wavelength of the injected light. In order to derive the hysteresis loop profile we calculate output photon density of the injected mode S_m from Eq. (6), by calculating A_m and B for n corresponding to each of two stable stationary points from the dn/dt versus n phase plot. The photon phase θ_m is then calculated from the stationary form of Eq. (4). In Figs. 1(b) and 1(c) we present dependencies of the output photon density S_m and phase θ_m on the P_{inj}, respectively. The stationary points which do not belong to the bistability region (as SP_1 and SP_3) map into the points outside of the hysteresis loops. The point SP_3 corresponding to low P_{inj} is settled on the left side of the loop, while the one corresponding to high P_{inj}, SP_1, is settled on the right side of the loop [dot-dashed lines in Figs. 1(b) and 1(c)].

By using Fig. 1 it is possible to follow the transition of the stationary points in the dn/dt versus n phase plot and their corresponding transition along the hysteresis loop in dependence on P_{inj}. If the P_{inj} is increased beyond -7.1 dBm, the SL slides from the SP_3 state into the $n_{sp}^{(3)}$ state, denoted as state 1. This state corresponds to the lower branch of the S_m [Fig. 1(b)], and the upper branch of the θ_m hysteresis [Fig. 1(c)]. Further increase in P_{inj} shifts the SL from the $n_{sp}^{(3)}$ state denoted as state 1, to $n_{sp}^{(3)}$ states denoted with higher numbers (2, 3) as long as $n_{sp}^{(3)}$ state exists, i.e., up to the $n_{sp}^{(3)}$ state denoted as state 3. Once P_{inj} overcomes -2.4 dBm, the dn/dt versus n phase plot again has only one stationary point with low operating carrier concentration [SP_1 in Fig. 1(a)], and SL jumps from the last $n_{sp}^{(3)}$ state provided (state 3) to this one. As mentioned earlier, this SP_1 state is mainly a consequence of injection locking, and due to the low operating carrier concentration, the central (dominant) mode is highly suppressed. The drive of the master laser in the reverse direction, corresponding to the decrease in P_{inj}, slides the SL into the $n_{sp}^{(1)}$ state (state 4), once P_{inj} again enters the bistability region. Further decrease in P_{inj} will keep the SL in the $n_{sp}^{(1)}$ state (e.g., points 4, 5 up to 6), as long as it is provided, i.e., up to $P_{inj} = -7.1$ dBm corresponding to point 6. In terms of the hysteresis loops, the $n_{sp}^{(1)}$ state corresponds to the upper branch of the S_m, and the lower branch of the θ_m hysteresis. Decreasing P_{inj} below $P_{inj} = -7.1$ dBm brings the SL back to the starting point SP_3, when only the state close to the free-running regime exists, thus completing a full hysteresis cycle.

In the region of the bistability, the SL will be stabilized in either the upper or the lower hysteresis branch, i.e., either in the $n_{sp}^{(1)}$ or the $n_{sp}^{(3)}$ state, depending on the laser prehistory. As shown in this case study, switching between the states (branches) can be achieved by variation of P_{inj}, which needs to temporarily overcome the boundaries defined by the hatched area in Fig. 1(a). In this way, the operating point is pushed out from one of the branches of the hysteresis loop, and then moved, i.e., switched to the opposite hysteresis branch, after P_{inj} is settled back to its previous value.

For the given laser structure and input parameters used in our computation, photon densities of injected signal and all longitudinal modes are smaller than 10^{15} cm^{-3}, which is at least two orders of magnitude smaller than the photon density necessary to trigger the mechanism of nonlinear gain suppression [16]. Therefore we neglect the nonlinear gain suppression in this work. However, preliminary investigation shows that the nonlinear gain suppression may become important in the case of higher bias currents, due to increased photon densities. In this case, it can cause shrinkage of the hysteresis width, which may affect the switching time and energy. A much deeper and more systematic numerical analysis of the bistability, hysteresis loops, and corresponding switching time and energy, with inclusion of all supported modes and nonlinear gain suppression mechanism, is required, and it will be provided in some future work.

IV. SWITCHING MODEL

We base our analysis of switching between bistable states on a simple analytical model [14]. However, since this model is based on several approximations of the full scale rate equation model, Eqs. (1)–(7), one could suspect that it lacks precision. Therefore, we tested the model by comparison with numerical simulations of the full scale rate equation model and found that analytical approach is sufficiently precise to estimate the switching time properly. In derivation of the analytical switching model, we assume that the stationary photon density can be reached much faster than the carrier density. The second assumption is that the carrier concentration n does not change considerably as the SL switches between $n_{sp}^{(1)}$ and $n_{sp}^{(3)}$ compared to the case of complete turn on and off. This assumption means that, depending on the switching direction, we may fix the total recombination rate $Q(n)$ to a value corresponding to some switching carrier concentration n_x between $n_{sp}^{(1)}$ and $n_{sp}^{(3)}$, i.e., $Q(n_x) = A_{SRH}n_x + R_{sp}(n_x) + C_A n_x^3$, which we chose according to the switching direction. Since the SL is stabilized in the initial state before the switching, the laser will remain in its vicinity most of the switching time. As the switching is over once the final state is just reached, one can conclude that an average carrier concentration during the switching is closer to the initial carrier concentration than to the final one. Therefore, for the case of switching from $n_{sp}^{(3)}$ to $n_{sp}^{(1)}$ it is justified to assume that n_x corresponds to the initial carrier concentration, i.e., $n_x = n_{sp}^{(3)}$, while in the reverse direction, following the same logic, n_x is set to $n_{sp}^{(1)}$. Finally, since the stationary point $n_{sp}^{(3)}$ is always lower than the FR threshold carrier concentration, we may assume that emission from unlocked modes will not have significant influence on the carrier rate equation, Eq. (1), as long as the carrier concentration $n \leqslant n_{sp}^{(3)} < n_{th}^{FR}$. This assumption is based on the results shown in [11] and mentioned in the previous section. It states that for carrier concentrations lower than n_{th}^{FR}, the maximum emission from the unlocked modes is considerably less intensive than the maximum emission from the IL mode. By that, we remove the necessity for unlocked modes photon rate equations in further consideration and neglect their contribution in the carrier rate equation. Indeed, the profile of the dn/dt versus n phase plot mainly depends on the IL mode m for a wide range of n except in the vicinity of n_{th}^{FR}. In contrast to our previous analysis [14] in which we assumed $n_{sp}^{(3)} = n_{th}^{FR}$, in this paper we keep original value for $n_{sp}^{(3)}$ corresponding to derived hysteresis loops obtained from the full scale rate equation model or more precisely, from Eqs. (6) and (7). Although all mentioned approximations reduce the accuracy of our model, they provide a possibility to analytically and more directly investigate the influence of α and N_w on the switching time and energy between the stable states. We start from Eq. (6), with the assumption that spontaneous emission term B in the photon density equation for the IL mode can be neglected. From Eq. (6), with $B = 0$, we derive stationary S_m and consequently θ_m [14]:

$$S_m = 4k_c^2 S_{inj}/\left[A_m^2(1+\alpha^2) - 4A_m\alpha\Delta\omega + 4\Delta\omega^2\right], \quad (8)$$

$$\theta_m = \arcsin\left[\frac{\alpha A_m - 2\Delta\omega}{\sqrt{A_m^2(1+\alpha^2) - 4\alpha\Delta\omega A_m + 4\Delta\omega^2}}\right]. \quad (9)$$

We further modify Eq. (1) in which we exclude the contribution of unlocked modes, keeping the IL mode, for which photon density S_m is given by Eq. (8) and fix contributions of radiative and nonradiative spontaneous recombination $Q(n_x)$:

$$dn/dt = I/(qV) - Q(n_x) - v_g g(n,\omega_m + \Delta\omega)S_m. \quad (10)$$

In Fig. 2, we show dn/dt versus n phase plots obtained from Eq. (10) for the same other input parameters as before, i.e., $\Delta\omega = -14\Omega$, $\alpha = 3$, and $N_w = 3$. It can be seen that the phase plots shown in Figs. 1 and 2 are slightly different, due to introduced approximations. The plots in Fig. 2 are obtained for P_{inj} corresponding to the limiting values of the bistability range, $P_{inj} = -6.6$ dBm ($n_{sp}^{(2)}$ merges with $n_{sp}^{(1)}$) and $P_{inj} = -2.2$ dBm ($n_{sp}^{(2)}$ merges with $n_{sp}^{(3)}$) and for the injection power $P_0 = -4.4$ dBm. The power P_0 corresponds to P_{inj} for which the $n_{sp}^{(1)}$ point lies in the middle of the carrier concentration range corresponding to the $n_{sp}^{(1)}$ bistability range, although it may look like it coincides with the average power of the bistability range as depicted in the left inset in Fig. 2. However, our calculation shows that there is negligible difference if P_0 is defined as the medium power of the bistability range. Figure 2 also provides the dn/dt versus n phase plot at injection power P_0, for all modes included (IL as well as unlocked modes), based on Eq. (1), which can be evaluated by the function given on the left side of Eq. (7) and for a fixed spontaneous recombination term $Q(n_x)$ (dot-dashed line in Fig. 2). It can be seen that this plot almost completely overlaps the one derived from Eq. (10) comprising only the IL mode. The difference occurs only in the vicinity of n_{th}^{FR} (cf. right inset in Fig. 2). It can be seen in the right inset of Fig. 2 that

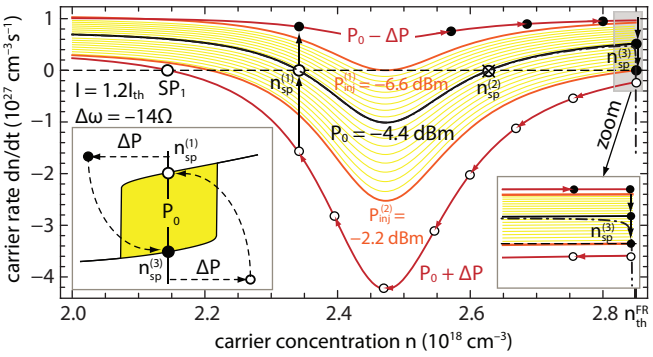

FIG. 2. (Color online) dn/dt versus n phase plots accounting only for the IL side mode $m=-5$ for $\Delta\omega=-14\Omega$, $\alpha=3$, $N_w=3$, and fixed total recombination rate $Q(n_x)$. The dot-dashed line represents the phase plot obtained for all modes included. The hatched area represents the area of multiple stationary points. Arrowed lines represent phase plots corresponding to switching powers $P_0\pm\Delta P$. Left inset: Schematic S_m hysteresis loop and trajectories of switching. Right inset: Enlarged vicinity of the $n_{sp}^{(3)}$ state.

dn/dt versus n phase plots corresponding to Eq. (10) do not cross the n axis, which would have happened, if the unlocked modes had been included in Eq. (10) as they were in Eq. (1). Nevertheless, the n coordinate of the right ending point of the phase plot obtained from Eq. (10) almost completely coincides with $n_{sp}^{(3)}$, which means that the negligence of the unlocked modes is justified with respect to the dn/dt versus n phase plot profile as long as the accurate position of $n_{sp}^{(3)}$ is known. In other words, if we use the simplified model represented by Eq. (10) in describing dn/dt versus n phase plots, the right ending point is equivalent and corresponds to $n_{sp}^{(3)}$. However, $n_{sp}^{(3)}$ has to be derived from the full scale rate equation model, or more precisely from Eq. (7), since Eq. (10) cannot provide it.

As explained before, we analyze the switching between stable points $n_{sp}^{(1)}$ and $n_{sp}^{(3)}$ and vice versa by variation of P_{inj}. In this analysis we focus on the points depicted in Fig. 2, which we obtain after simplifications imposed by the approximations of the model. This means that we start from P_{inj} set to P_0 for which the SL is either in the $n_{sp}^{(1)}$ (upper hysteresis branch) or in the $n_{sp}^{(3)}$ state (lower hysteresis branch; cf. left inset in Fig. 2). In order to switch from $n_{sp}^{(3)}$ to $n_{sp}^{(1)}$, P_{inj} needs a variation (ΔP), i.e., it has to be rapidly increased to some $P_{inj}=P_0+\Delta P>P_{inj}^{(2)}$ which corresponds to the case when only one (SP_1) steady state appears (lower arrowed line in Fig. 2). This power overcomes the hysteresis edge ($P_{inj}^{(2)}$) and corresponds to the upper right tail of the hysteresis. If this power ($P_{inj}=P_0+\Delta P$) is kept fixed for some short time interval, SL will begin to gradually slide toward the only steady state provided. When P_{inj} is returned back to P_0, instead of stabilizing in the SP_1 state, SL switches to $n_{sp}^{(1)}$ and completes the switching. In the reverse process, in order to switch from $n_{sp}^{(1)}$ to $n_{sp}^{(3)}$, P_{inj} has to be decreased to some $P_{inj}=P_0-\Delta P<P_{inj}^{(1)}$, corresponding to the case when only SP_3 appears (upper arrowed line in Fig. 2). Here $P_{inj}^{(1)}$ represents the lower hysteresis edge. This power is kept fixed for some short time interval while SL slides toward SP_3, and when the power is returned back to P_0, laser stabilizes in the $n_{sp}^{(3)}$ state. In this case the operating point of the SL is switched from the upper branch of the hysteresis to the lower one. In order to derive expression for switching time calculation we rewrite Eq. (10) with respect to $A=A_m$ [14]:

$$dn/dt=\xi dA/dt=Q_{net}-\left(A+\tau_p^{-1}\right)S_m/\Gamma. \tag{11}$$

In Eq. (11) $Q_{net}=I/(qV)-Q(n_x)$ is the effective rate of the carrier injection into the SL, depending on the bias current $I=1.2I_{th}$, and total recombination rate Q with respect to the switching carrier concentration n_x, while $\xi=[\Gamma v_g(dg/dn)]^{-1}$. Equation (11) can be rewritten in the following form [14]:

$$\xi\left[Q_{net}^{-1}+(K_4A+K_5)(K_1A^2+K_2A+K_3)^{-1}\right]dA=dt. \tag{12}$$

Definite integration of Eq. (12) gives

$$\begin{aligned}t_{if}=&\frac{\xi(A_f-A_i)}{Q_{net}}+\frac{\xi K_4}{2K_1}\ln\left(\frac{K_1A_f^2+K_2A_f+K_3}{K_1A_i^2+K_2A_i+K_3}\right)\\&+\frac{\xi(2K_1K_5-K_2K_4)}{K_1\sqrt{4K_1K_3-K_2^2}}\\&\times\arctan\left[\frac{(A_f-A_i)\sqrt{4K_1K_3-K_2^2}}{2K_1A_fA_i+K_2(A_f+A_i)+2K_3}\right].\end{aligned} \tag{13}$$

The definite integral given by t_{if} represents the switching time between the initial $A_m=A_i$ and the final $A_m=A_f$ state, where i stands for 1 or 3, i.e., corresponds to $n_{sp}^{(1)}$ or $n_{sp}^{(3)}$, while f stands for 3 or 1, i.e., $n_{sp}^{(3)}$ or $n_{sp}^{(1)}$. Furthermore, $K_1=Q_{net}^2\Gamma\tau_p(1+\alpha^2)$, $K_2=-4Q_{net}\tau_p(Q_{net}\alpha\Gamma\Delta\omega+k_c^2S_{inj})$, $K_3=4Q_{net}(Q_{net}\Gamma\Delta\omega^2\tau_p-k_c^2S_{inj})$, $K_4=4k_c^2S_{inj}\tau_p$, and $K_5=4k_c^2S_{inj}$. In these expressions, S_{inj} corresponds to $P_{inj}=P_0\pm\Delta P$.

From Eqs. (6) and (7) and for known $\Delta\omega$ we calculate the range of P_{inj} for which the bistability occurs, i.e., the hysteresis edges ($P_{inj}^{(1)}$ and $P_{inj}^{(2)}$), the corresponding starting power (P_0), as well as carrier concentrations for switching states $n_{sp}^{(1)}$ and $n_{sp}^{(3)}$ within the hysteresis loops. Stimulated photon generation rates, corresponding to these states, are given by $A_m(n_{sp}^{(1)})=\Gamma v_g g(n_{sp}^{(1)},\omega_m+\Delta\omega)-\tau_p^{-1}$ and $A_m(n_{sp}^{(3)})=\Gamma v_g g(n_{sp}^{(3)},\omega_m+\Delta\omega)-\tau_p^{-1}$. Depending on a desired direction of the switching, one of these states represents the initial state, and the other one is the final state. Finally, with S_{inj} corresponding to $P_{inj}=P_0\pm\Delta P$, by using Eq. (13), we calculate the switching time t_{if} between the states with respect to the variation of injection power ΔP. Since the loops derived from the full scale rate equation model, Eqs. (1)–(7), are slightly different than the loops derived directly from the simplified analytical model, Eqs. (8)–(10), we adopt ΔP which is large enough to compensate for this small difference and to enable the analytical model to remain on the safe side. The switching energy is finally calculated as $E_{if}=\Delta P t_{if}$.

V. RESULTS AND DISCUSSION

The analysis in the paper is focused on the influence of the linewidth enhancement factor α, and the number of quantum wells N_w in the SL active region on the switching time between bistable states and the corresponding switching energy. The linewidth enhancement factor α is of great importance for injection locking properties and, as shown in [12], affects the locking range and stability of the IL lasers. Here we show that α also affects the width and the general profile of the hysteresis loops and thus, indirectly the time and energy of switching between the stable states. Although we can account for the carrier-dependent refractive index variation spectrum [17], as well as the dispersive linewidth enhancement factor, in this study we assume that the linewidth enhancement factor is nondispersive and independent of the carrier density and gain spectrum. This assumption is motivated by the fact that the value of the linewidth enhancement factor affects only the injection-locked mode. For this particular mode, the frequency detuning is in the order of intermodal spacing, which is generally insufficient to cause significant variation of the linewidth enhancement factor as well as the refractive index. Moreover, the switching between stable states corresponds to low variation of carrier density, which supports negligence of α factor variation with carrier density. Although different nondispersive α factors generally correspond to different gain spectra, we investigate the influence of the linewidth enhancement factor by using two fixed values of α for the same gain spectrum. This approach provides us better insight into the shear influence of the α factor on the hysteresis profiles and switching times between bistable states. Moreover, it can be seen that K_1 and K_2 in Eq. (13) depend on α and directly affect the switching. On the other hand, the number of quantum wells N_w is directly proportional to the SL confinement factor Γ. Since ξ is inversely proportional to Γ, an increase in N_w leads to the decrease in ξ. The decrease in ξ does not directly affect the first term in Eq. (13) since its decrease is compensated by the increase in $A_m(n_{sp}^{(1)})$ and $A_m(n_{sp}^{(3)})$, which linearly increase with Γ. However, the other two terms in Eq. (13) are proportional to ξ and decrease with it. The other parameters K_1, K_2, and K_3 also depend on Γ, but affect Eq. (13) in a nontrivial way. In addition to this, the increase in N_w leads to the increase in the SL active volume, which causes the decrease in Q_{net}. On the other hand, the increase in Γ reduces the free-running threshold carrier concentration n_{th}^{FR} and consequently the threshold current I_{th}. In the case of the fixed ratio of the applied and threshold current ($I/I_{th} = 1.2$), the applied current decreases as the threshold current, which together with the increase in V lead to an inevitable decrease in Q_{net}. Similarly to Γ, Q_{net} also affects K_1, K_2, and K_3 leading to complex dependence of t_{if} on the active region volume V.

According to the previous analysis, it is clear that α and N_w represent very important parameters in terms of IL laser switching dynamics. In order to study their influence, we investigate t_{if} and the corresponding E_{if} for two values for each of these parameters, providing four possible combinations for ordered pair $\{\alpha, N_w\}$. In the analysis we assume $\alpha = 3$ [18] or 6 [19] and $N_w = 3$ ($n_{th}^{FR} = 2.85 \times 10^{18}$ cm^{-3}, $I_{th} = 8.16$ mA) or $N_w = 6$ ($n_{th}^{FR} = 1.88 \times 10^{18}$ cm^{-3}, $I_{th} = 6.25$ mA). Apart from that, as we perform switching with P_{inj} variation, we analyze the influence of the frequency detuning on t_{if} and the corresponding E_{if}.

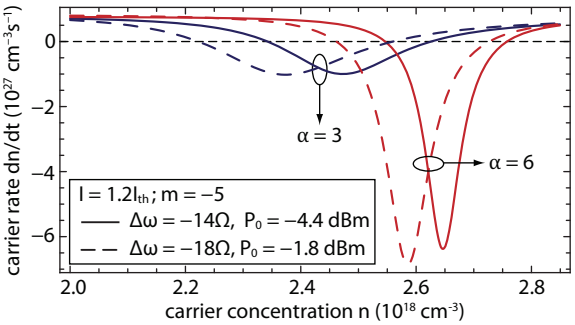

FIG. 3. (Color online) dn/dt versus n phase plots in the case of $N_w = 3$, for two values of α and $\Delta\omega$, with P_{inj} set to P_0 for a given value of α and $\Delta\omega$.

In Fig. 3 we present a family of dn/dt versus n phase plots obtained for two different values of α ($\alpha = 3,6$) and $\Delta\omega$ ($\Delta\omega = -14\Omega, -18\Omega$). The phase plots are calculated by using Eqs. (10) and (8), for $N_w = 3$ and $m = -5$. It can be seen that in phase plots obtained for higher values of α, $n_{sp}^{(1)}$ is shifted toward n_{th}^{FR}, meaning that the $n_{sp}^{(1)}$ and $n_{sp}^{(3)}$ states are closer to each other, compared to the case of phase plots obtained for the lower values of α. The reason for this is related to Eq. (8) which changes more rapidly with the carrier concentration n for higher values of α. The rapid change occurs due to the reduced opening of the parabola in the denominator of Eq. (8), which becomes narrower with the increase in α. The proximity of the initial and the final stationary point for higher α leads to the reduction of the linear and other two terms in Eq. (13) and the corresponding switching time. In addition to this, the maximum of the denominator in Eq. (8) occurs for $A_m = 2\alpha\Delta\omega/(1+\alpha^2)$. This means that for the more negative detuning $\Delta\omega$, A_m becomes more negative, which corresponds to the lower carrier concentration. Thus one can see that the phase plots for the same values of α, shift toward the lower carrier density as $\Delta\omega$ becomes more negative. As can be seen in Fig. 3, for a fixed $\Delta\omega$ and P_{inj}, higher α leads to larger bending of the dn/dt versus n phase plot, which means that bistability can be provided by lower P_{inj} than in the case of the lower linewidth.

In Fig. 4 we present photon density S_m as a function of P_{inj}, for different values of α, N_w, and $\Delta\omega$. Although the results in Fig. 4 are derived from the full rate equation model and Eqs. (6) and (7), their analysis can be based on simplified Eq. (6), i.e., on Eq. (8). It can be seen that higher α leads to the lower S_m for higher branches of the hysteresis loops. Due to an increase in α, the denominator in Eq. (8) also increases. As shown in Fig. 3, higher α leads to larger $n_{sp}^{(1)}$, which corresponds to lower negative A_m, i.e., low $|A_m|$ (or gain defect). Although low, $|A_m|$ is not low enough to significantly reduce the increase of the denominator in Eq. (8), which consequently leads to a low output photon density S_m. However, a lower S_m is not a problem for bistability in the case of high linewidth, since the bending of the phase plot is significant, as previously discussed and shown in Fig. 3. The range of P_{inj} for which hysteresis loops occur, and corresponding switching time and energy, are also dependent on the frequency detuning $\Delta\omega$.

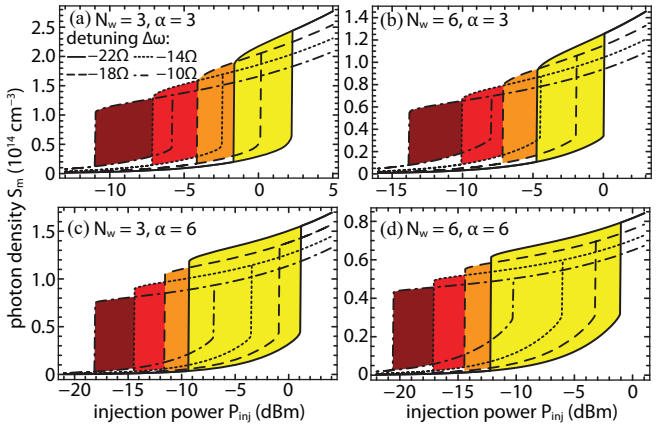

FIG. 4. (Color online) Photon density S_m versus $P_{\rm inj}$ hysteresis loops for different values of $\Delta\omega$ (-22Ω, solid line; -18Ω, dashed line; -14Ω, dotted line; -10Ω, dot-dashed line) for $\{N_{\rm w},\alpha\}$ taking values (a) $\{3, 3\}$, (b) $\{6, 3\}$, (c) $\{3, 6\}$, and (d) $\{6, 6\}$.

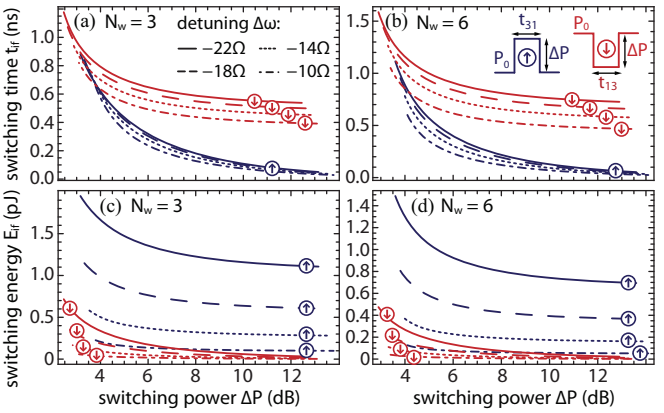

FIG. 5. (Color online) Switching time for (a) $N_{\rm w} = 3$ and (b) $N_{\rm w} = 6$, and switching energy for (c) $N_{\rm w} = 3$ and (d) $N_{\rm w} = 6$, for $\alpha = 3$ and different values of $\Delta\omega$ in cases of power increase (switching from $n_{\rm sp}^{(3)}$ to $n_{\rm sp}^{(1)}$; curves with arrow up) and power decrease (switching from $n_{\rm sp}^{(1)}$ to $n_{\rm sp}^{(3)}$; curves with arrow down).

As in the previous case, the more negative $\Delta\omega$ increases the denominator in Eq. (8), leading to lower S_m corresponding to the upper branch of the hysteresis loop. Low S_m may lead to an insufficient bending of the dn/dt versus n phase plot and interruption of the bistability regime. The way to compensate for S_m decrease and to keep the SL in the bistability regime is to increase the injection photon density $S_{\rm inj}$, i.e., $P_{\rm inj}$. This means that more negative $\Delta\omega$ shifts the loops towards higher $P_{\rm inj}$ (cf. Fig. 4), resulting in the higher switching energy. Moreover, the higher density of injected photons in the case of more negative $\Delta\omega$ means that $n_{\rm sp}^{(1)}$ is shifted towards lower values, thus $n_{\rm sp}^{(1)}$ and $n_{\rm sp}^{(3)}$ are more separated (cf. Fig. 3) leading to larger difference $A_f - A_i$. This difference increases all three terms in Eq. (13), which lead to a longer switching time. Finally, an increase in $N_{\rm w}$ and consequently in V and Γ, lowers the value of the gain threshold, the number of supported modes, and $n_{\rm th}^{\rm FR}$. Since the SL operates at lower carrier concentrations, the output photon densities of all modes are lower, while the injection locking needs lower $P_{\rm inj}$ to achieve locking of a particular side mode. In terms of the laser bistability, this means that hysteresis loops, obtained for higher $N_{\rm w}$, have lower S_m densities, and that the loops are shifted toward lower values of injection power (cf. Fig. 4). Since hysteresis loops appear at lower values of $P_{\rm inj}$, it can be expected that less energy has to be employed in order to switch between the hysteresis branches. In addition to this, due to the lower $n_{\rm th}^{\rm FR}$, the threshold current is lower. For a fixed $I/I_{\rm th}$ ratio, the decrease in the threshold current and the increase in the active region volume lead to the lower well pumping, i.e., a decrease in the $I/(qV)$ term in Eq. (10). The lower bias current I, in combination with smaller carrier concentration for higher $N_{\rm w}$, lowers the value of the effective rate for the carrier injection $Q_{\rm net} = I/(qV) - Q(n_{\rm x})$ in Eq. (11). This directly leads to a longer switching time, since it dominantly increases the value of the integral given by Eq. (13).

In Fig. 5 we present calculated switching time and energy versus the variation of injection power (ΔP), measured from the starting injection power P_0, for a relatively low adopted value of $\alpha = 3$ and two different numbers of quantum wells, $N_{\rm w} = 3$ and $N_{\rm w} = 6$. Figure 5 shows the switching time and energy in the case of power increase (switching from $n_{\rm sp}^{(3)}$ to $n_{\rm sp}^{(1)}$) and power decrease (switching from $n_{\rm sp}^{(1)}$ to $n_{\rm sp}^{(3)}$) for different values of $\Delta\omega$. It should be mentioned that the same variation of the injection power, ΔP, expressed in dB, corresponds to different values of power variation expressed in SI units for switching in opposite directions. In other words, $+\Delta P$ represents a larger power variation than $-\Delta P$, assuming the same P_0. Moreover, a decrease in P_0 leads to even smaller power variations for the fixed ΔP and usually means lower switching energy. In calculation of $t_{\rm if}$ and $E_{\rm if}$ we apply expression (13) derived in Sec. IV. It can be seen that switching from $n_{\rm sp}^{(1)}$ to $n_{\rm sp}^{(3)}$ lasts longer than the reverse process, but due to lower $P_{\rm inj}$ it has lower switching energy. With an increase in $N_{\rm w}$, switching time increases, but switching energy becomes lower due to the decrease in the effective rate of the carrier injection $Q_{\rm net}$. In addition to this, more negative $\Delta\omega$, as we already explained, leads to larger separation of the stationary points, and consequently to longer switching time and higher switching energy. In the case of switching by $P_{\rm inj}$ decrease, switching energies for higher values of $N_{\rm w}$ and less negative $\Delta\omega$ can be very low, in the order of 10 fJ, though corresponding switching times are in the order of 0.5 ns.

In Fig. 6 we present calculated switching time and corresponding energy for $\alpha = 6$ in cases of $N_{\rm w} = 3$ and $N_{\rm w} = 6$. Figure 6 clearly shows lower switching time in comparison with Fig. 5. However, this comparison does not take into account the width of the hysteresis loops, which are wider for larger values of the linewidth. In order to provide a fair comparison for $\alpha = 3$ and $\alpha = 6$, we can define ΔP as the power variation counted from the hysteresis edge, rather than from its middle, and compare switching times for the same level of power variation ΔP to learn that switching times for $\alpha = 6$ are indeed shorter than those for $\alpha = 3$. In addition to this, an increase in α leads to a more energy efficient switching [Figs. 6(c) and 6(d)]. The reason for this lies in the shorter switching time, and the fact that hysteresis loops are shifted toward lower $P_{\rm inj}$. In the case of $\alpha = 6$, $N_{\rm w} = 6$, and $\Delta\omega = -10\Omega$ [dot-dashed line in Fig. 4(d)], small signal stability analysis [12] shows that the $n_{\rm sp}^{(3)}$ branch of the

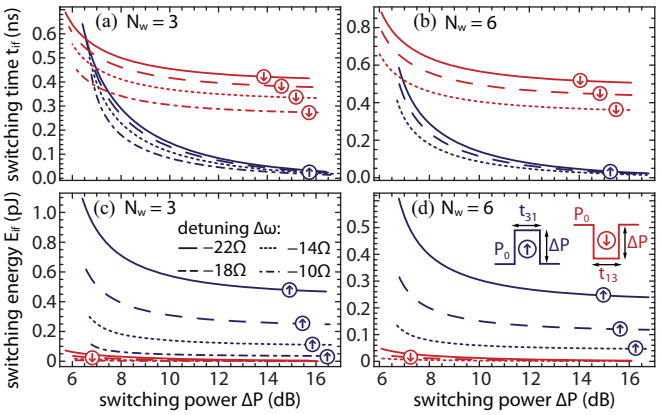

FIG. 6. (Color online) Switching time for (a) $N_w = 3$, and (b) $N_w = 6$, and switching energy for (c) $N_w = 3$, and (d) $N_w = 6$, for $\alpha = 6$ and different values of $\Delta\omega$ in cases of power increase (switching from $n_{sp}^{(3)}$ to $n_{sp}^{(1)}$; curves with arrow up) and power decrease (switching from $n_{sp}^{(1)}$ to $n_{sp}^{(3)}$; curves with arrow down).

hysteresis loop is not stable, thus the switching between $n_{sp}^{(1)}$ and $n_{sp}^{(3)}$ does not occur. Our model shows that for sufficiently large ΔP, with high values of α, switching time can be very short, even shorter than 10 ps [c.f. Fig 6(a)]. However, in such cases, due to large ΔP, switching energy is high, in the order of 100 fJ [cf. Fig. 6(c)]. In the process of switching with power decrease, due to low values of P_{inj}, switching energy can be even lower than 1 fJ, but on account of the longer switching time which is in the order of 0.4 ns. The conducted analysis shows that both switching time and energy significantly depend on the switching direction. Although the switching time for the opposite directions becomes comparable for small ΔP, it is generally long, since it is in the order of 0.5 ns. On the other hand, the switching energy can be comparable for a wide range of ΔP, especially for low-frequency detuning. A future investigation should study a possibility to decrease the switching energy, as well as balancing the switching time and energy with respect to the switching direction.

VI. CONCLUSION

In this paper we analyze the influence of the linewidth enhancement factor and the active region volume on the switching properties of the IL bistable Fabry-Perot lasers. From the full scale model of the IL laser rate equations, we calculate hysteresis loops and derive a simple analytical model for calculation of the switching time and corresponding energy with respect to P_{inj} and $\Delta\omega$. We show that the higher values of linewidth enhancement factor α reduce switching time and switching energy, since higher values of α bring switching states closer with respect to their carrier concentrations. Moreover, hysteresis loops are shifted toward lower values of P_{inj}, making switching more energy efficient. Increase in the active region volume, can also lead to lower switching energy since the laser gain threshold is lower. However, this causes the switching time to become longer, as a result of the lower value of the effective rate of carrier injection, which dominantly increases the switching time. In addition to this, we show that switching characteristics also depend on the frequency detuning. A less negative $\Delta\omega$ leads to better switching characteristics, i.e., lower switching time and energy, since switching states are closer with respect to the carrier concentration, while the hysteresis loops are shifted toward lower P_{inj}.

ACKNOWLEDGMENTS

This work was supported by the Serbian Ministry of Education and Science (project Photonics Components and Systems 171011).

[1] W. Coomans, S. Beri, G. Van der Sande, L. Gelens, and J. Danckaert, Phys. Rev. A **81**, 033802 (2010).
[2] L. Olejniczak, K. Panajotov, H. Thienpont, and M. Sciamanna, Phys. Rev. A **82**, 023807 (2010).
[3] N. Kashima, S. Yamaguchi, and S. Ishii, J. Lightwave Technol. **22**, 550 (2004).
[4] J. W. Wu and Y. H. Won, J. Opt. **15**, 075502 (2013).
[5] A. Hurtado, M. Nami, I. D. Henning, M. J. Adams, and L. F. Lester, IEEE J. Sel. Top. Quantum Electron. **19**, 1900708 (2013).
[6] S. Osborne, K. Buckley, A. Amann, and S. O'Brien, Opt. Express **17**, 6293 (2009).
[7] N. L. Hoang, J. S. Cho, Y. H. Won, and Y. D. Jeong, Opt. Express **15**, 5166 (2007).
[8] K. Hybrechts, T. Tanemura, K. Takeda, Y. Nakano, R. Baets, and G. Morthier, IEEE J. Sel. Top. Quantum Electron. **16**, 1434 (2010).
[9] M. C. Pochet, N. A. Naderi, V. Kovanis, and L. F. Lester, IEEE J. Quantum Electron. **47**, 827 (2011).
[10] K. Hybrechts, W. D'Oosterlinck, G. Morthier, and R. Baets, IEEE Photonics Technol. Lett. **20**, 18 (2008).
[11] M. Krstić, J. Crnjanski, and D. Gvozdić, IEEE J. Sel. Top. Quantum Electron. **18**, 826 (2012).
[12] M. Krstić, J. Crnjanski, M. Mašanović, L. Johansson, L. Coldren, and D. Gvozdić, IEEE J. Sel. Top. Quantum Electron. **19**, 1501408 (2013).
[13] R. Lang, IEEE J. Quantum Electron. **18**, 976 (1982).
[14] D. Gvozdić, M. Krstić, and J. Crnjanski, Opt. Lett. **36**, 4200 (2011).
[15] R. Hui, J. Lightwave Technol. **13**, 42 (1995).
[16] L. Coldren, S. Corzine, and M. Mašanović, *Diode Lasers and Photonic Integrated Circuits* (Wiley-Interscience, New York, 2012).
[17] A. R. Totović, J. V. Crnjanski, M. M. Krstić, M. L. Mašanović, and D. M. Gvozdić, IEEE J. Sel. Top. Quantum Electron. **19**, 3000411 (2013).
[18] E. Lau, H. K. Sung, and M. C. Wu, IEEE J. Quantum Electron. **44**, 90 (2008).
[19] C. Henry, IEEE J. Quantum Electron. **18**, 259 (1982).